Journal of Geoscience and Environment Protection, 2024, 12, 107-130
https://www.scirp.org/journal/gep
ISSN Online: 2327-4344
ISSN Print: 2327-4336

Petrology and Geochemical Relationship of Birimian Gabbro-Diorite-Granodiorite Dykes in Basaltic Rocks at Butre Area, SW Ghana

Victor Graham, George Mensah Tetteh

Department of Geological Engineering, University of Mines and Technology, Tarkwa, Ghana
Email: gmtetteh@umat.edu.gh

How to cite this paper: Graham, V., & Tetteh, G. M. (2024). Petrology and Geochemical Relationship of Birimian Gabbro-Diorite-Granodiorite Dykes in Basaltic Rocks at Butre Area, SW Ghana. *Journal of Geoscience and Environment Protection, 12,* 107-130.
https://doi.org/10.4236/gep.2024.122007

Received: November 9, 2023
Accepted: February 26, 2024
Published: February 29, 2024

Abstract

Granitoids at Butre area, south-western part of the Birimian of Ghana are gabbro to granodiorite which intruded comagmatic basalt and andesite of volcanic island arc setting. Differentiation was from probably mantle fractionates on tholeiitic basalt trend through gabbro-diorite and granodiorite. Yet, the diorite intruded into the volcanic rocks prior to plate collision. Plagioclase feldspars of labradorite to andesine compositions (An_{52} - An_{48}), amphibole and pyroxene are in association with accessory tourmaline, actinolite, apatite and garnet. Relict amphibolite facies metamorphism is preserved in xenoliths in gabbro to diorite which show greenschist facies. Generally, plagioclase is partially altered to fine quartz, sericite and carbonates whereas chlorite and epidote are of amphibole alteration. These alterations are typical of carbonatisation but diorite shows partial carbonate-sericite alteration. Alterations followed granodiorite emplacement. Arsenopyrite and pyrite accompanied emplacement of diorite and granodiorite respectively while amphibolite facies metamorphism introduced magnetite; haematite and pyrrhotite accompanied greenschist facies metamorphism. Earlier opaque minerals possibly were consumed to form later minerals. All the rocks are LREE depleted (La/Sm chondrite normalised ratios of basalt = 0.8 to 2.5; andesite = 2.03; diorite = 1.95 to 3.1; gabbro-diorite = 0.9 to 2.05; granodiorite = 1.66); diorite, basalt and andesite are fairly enriched in HREE. Enrichment of FeO_T, MgO, SiO_2, CaO and depletion of TiO_2, K_2O and Zr might be linked with carbonitisation, sericitisation, chloritisation, silicification and sulphidation linked to gold mineralisations in the Birimian of Ghana.

Keywords

Granitoids, Petrography, Alteration, Metamorphism, Geochemistry, Butre

1. Introduction

Granitoids in contact with host rocks are associated with different types of hydrothermal alterations. Example Irizar granite of Kukri Hills, Antarctica which was intruded by dolerite intrusives showed biotite altered to chlorite; and hornblende to chlorite and haematite (Craw & Findlay, 1984). At Galore Creek of Canada, diorite/monzonite intruded into sandstone, siltstone and chert and introduced hydrothermal potassic-calcic alterations (Micko et al., 2014). In the Tavsanlı area in Turkey, the Egrigöz granitoids intrusion into various gneisses and schists caused silicification, argillic-sillicic, and phyllic alterations along fault/shear zones at the contacts of granitoids (Kumral et al., 2016). In India, Rajastan, metavolcanic rocks intruded by granitoids have undergone mineralogical changes: oligoclase to albite, and biotite to annite, while rocks unaffected by hydrothermal activities remain intact (Kaur et al., 2012). Oxides of Si, Al, Na, K, Mg, Mn, Ca and Fe were encountered. Si_2O wt. % varies inversely to oxides of Al, Mg, Mn, Ca and Fe but almost directly to that of K_2O (Rajah et al., 1977).

The Birimian is a portion of the Man Shield, located south of the West African craton, comprising basins of metasedimentary rocks (commonly slates, phyllites, greywacke) disconnected by belts metavolcanic rocks (basalt, andesite, agglomerates, tuff) (Leube et al., 1990). The age of the Birimian as estimated from zircons in the metavolcanic rocks of the Birimian Supergroup shows ages between 2162 ± 6 Ma and 2266 ± 2 Ma, while detrital zircon grains from the metasedimentary rocks gave ages between 2180 and 2130 Ma (Oberthür et al., 1998; Perrouty et al., 2012). Three main types of granitoids are identified within the Birimian - sedimentary type (Cape Coast), volcanic belt type (Dixcove) and K-rich (Bongo) granitoid types (Hirdes et al., 1992). Minerals of the volcanic belt type are non-foliated quartz and hornblende diorite, while K-rich granitoids are associated with hornblende and microcline which are also non-foliated (Kesse, 1985). However, the sedimentary basin type is associated with well foliated marked by biotite, microcline, beryl etc. characterised by schist and gneiss enclaves (Perrouty et al., 2012). The belt type and basin type granitoids in Ghana were emplaced at different times (Leube et al., 1990). Loh & Hirdes (1999) stated that the age of belt granitoids in the southern portion of the Ashanti belt constrains those of the metavolcanic rocks and so are comagmatic with ages between 2145 - 2190 Ma, while the basin-type is regarded as late-to-post-kinematic and predates the Tarkwaian with ages between 2090 - 2125 Ma (Oberthür et al., 1995).

At Mpohor area, SE of the Ashanti belt, intrusions have led to the chloritisation of gabbro and diorite (Tetteh & Effisah-Otoo, 2017). Also at the Prestea mine, SW of the Ashanti belt, alteration of pyrite to marcasite is common (Perrouty et al., 2012) while at Bekpong area, NW Ghana, intrusions have led to the chloritisation and sericitisation of shale (Amponsah et al., 2016). Mineralisation includes Au deposits (Salvi et al., 2015; Allibone et al., 2004; Perrouty et al., 2012). Within the Birimian, hydrothermal mineralisation in the basin granitoids

is characterised by alterations of quartz, sericite, calcite etc. assemblage but alterations diminish away from mineralised zones with albite, pyrite, chlorite assemblage (Smith et al., 2016). Alteration halos of phyllite/basin type granitoid contact at Obuasi mine is smaller (Yao & Robb, 2000) compared to that of the basalt and volcanic sediments in contact with K-rich granitoids at the Julie deposit of Wa-East District (Amponsah et al., 2015). Tarkwaian Group overlies the Birimian rocks of the Ashanti belt (Eisenlohr & Hirdes, 1992) as clastic sediments that were deposited at an approximated constrained age between 2102 and 2097 Ma (Perrouty et al., 2012).

Three granitoids namely, tonalite in the south, granodiorite in the centre and gabbro/norite at the northern part of Mpohor town occur near metavolcanic rocks at Butre with xenoliths present in tonalite considered as contact metamorphosed, metasomatised basaltic rocks (Loh & Hirdes, 1999). The alterations and textures related to geochemistry of the granitoids and metavolcanic rocks have not been studied. This study therefore explored the geochemical relationship between the intrusives and their host metavolcanic rocks (**Figure 1**).

2. Geological Setting

2.1. Regional Geology

The West African craton is represented by rocks of lower Proterozoic timespan from 2500 to 1800 Ma. To the southernmost region lies the Man shield, made up largely of rocks of early Proterozoic age (Wright et al., 1985). The Man shield is made up of Archean rocks of Liberian age (3.0 - 2.5 Ga) which lies to the west and eastern portion made up of rocks of early Proterozoic age known as the Birimian rocks (Leube et al., 1990). To the southeastern portion of the Man shield, the Birimian rocks outcropextensively in La Côte d'Ivoire, Burkina Faso, western Ghana, southern Mali, west of Niger and Senegal (Abouchami et al., 1990).

The Birimian of the Man shield has been folded, metamorphosed and intruded by various pluton suites (granitoids) and is believed to have occurred during the Eburnean age at 2.1 Ga (Leube et al., 1990). The Birimian rocks of Ghana are composed of belts of metavolcanic rocks that have been disconnected by basins of sedimentary rocks (Leube et al., 1990). The metasedimentary rocks of the Birimian are commonly made up of slates, phyllites, metagreywacke, tuffaceous shale, siltstone and Mn rich chemical sedimentary rocks (Eisenlohr & Hirdes, 1992). The metavolcanic rocks on the other hand are made up chiefly of basalt and andesite with interflow of some pyroclastic rocks (Loh & Hirdes, 1999). In Ghana, the Birimian metasedimentary basins are located at the south-central (Cape Coast basin), southwestern (Kumasi and Sunyani basins) and the northern (Maluwe) respectively (Smith et al., 2016). Marginal to the belts are found various sedimentary rocks including wacke, turbidites, volcaniclastics, chemical sediments etc. (Hirdes et al., 1993). In general, the Birimian metasedimentary rocks progress into each other and divided into volcaniclastic rocks, turbidite related wacke, argillitic rocks and chemical sediments (Leube et al.,

1990).

Birimian metavolcanic belts also known as the greenstone belts strike almost parallel to each other in a southwesterly to northeasterly direction and covers hundreds of kilometers. From Griffis et al. (2002), the belts have approximated widths of 20 to 70 km for larger belts and 10 to 20 km for smaller belts, which mostly occur in the north. There were previously six belts in the Birimian of Ghana (Leube et al., 1990). However, Smith et al. (2016) outlined the following, named from southeast to northwest, Kibi-Winneba Belt; Ashanti Belt; Manso-Nkwanta-Asankragwa Belt; Sefwi Belt; Bui Belt; Bole-Navrongo Belt; Wa-Lawra Belt and Julie Belt as the major belts in Ghana. Tholeiitic lavas mostly of metamorphosed basalts and andesites are common within the belts together with some mafic rocks and interbedded dacite, rhyodacite and pyroclastics (Berge, 2011). Although lava/pyroclastic ratios are variable amongst the belts of the Birimian in Ghana, the highest ratios are observed in the Ashanti Belt whiles it is least in the Sefwi Belt (Leube et al., 1990).

In Ghana, the Tarkwaian Group overlies the Birimian rocks and is perceived as fragments of the Birimian that uplifted and eroded after the Eburnean Tectono-Thermal Event (Eisenlohr & Hirdes, 1992). The Tarkwaian is much matured within the Ashanti and the Bui Belts with approximated thickness of 2500 and 9000 m, respectively (Griffis et al., 2002).

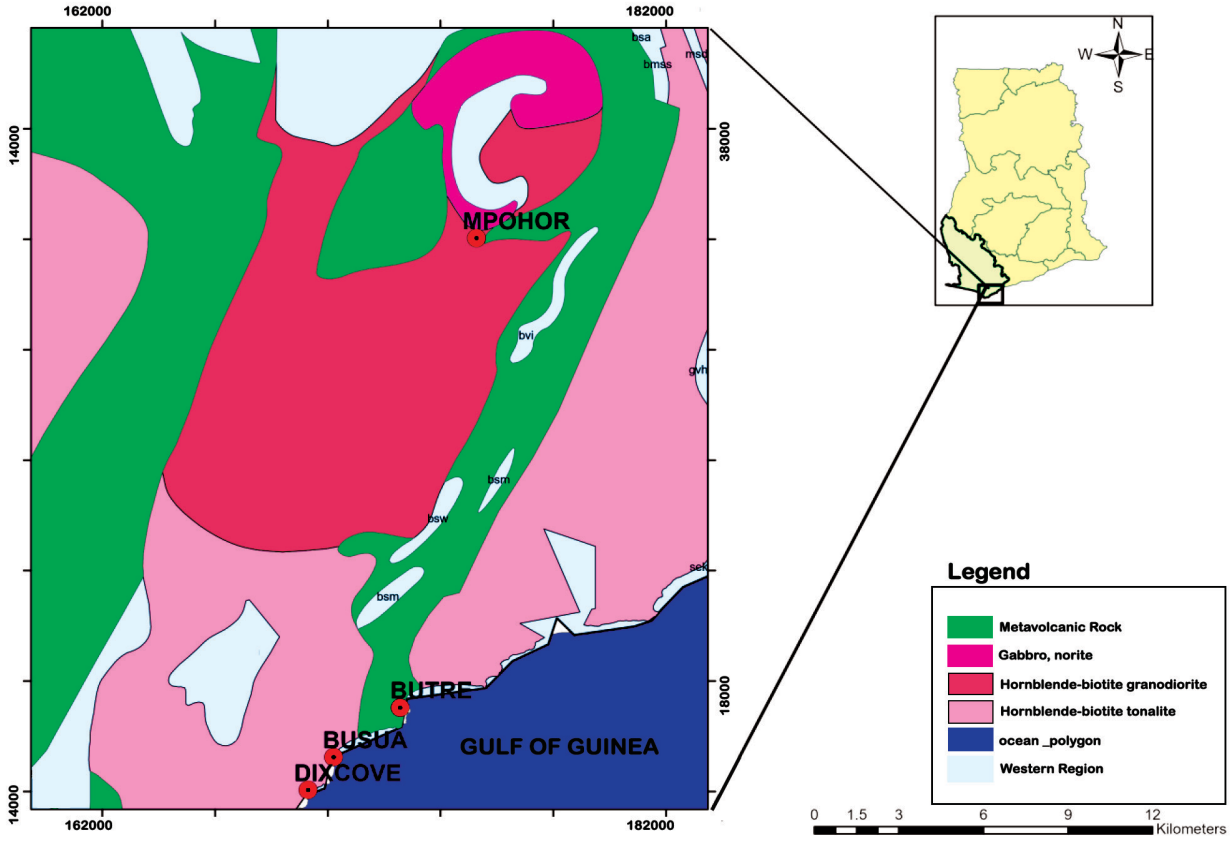

Figure 1. Geological map of SW Ghana showing study area.

2.2. Local Geology

Butre area lies on the far south of Ashanti Belt within the Birimian metavolcanic portion (**Figure 1**). This part of the belt is composed of volcanic rocks of mainly metamorphosed basalt and andesite together with pyroclastics and sedimentary rocks and have been intruded by granite-diorite suites (Dampare et al., 2008). There also occur mafic-ultramafic intrusives of various sizes, the largest having been described by Attoh et al. (2006) as complex ophiolite of Paleoproterozoic age and occurs in a supra-subduction zone. At Butre area, the metavolcanic rocks of the Birimian include pillow basaltic lavas. These rocks are in contact with three granitoids namely: tonalite in the south, granodiorite in the centre and gabbro/norite at the northern part of Mpohor town. Xenoliths present in tonalite are considered to be contact metamorphosed, metasomatised basaltic rocks (Loh & Hirdes, 1999). Metamorphism to amphibolite facies was observed in the rocks especially at areas in proximity to granitoids (John et al., 1999).

3. Methods Used

The area was mapped and locations determined using GPS and rocks described in hand specimen. Thirteen (13) representative samples were selected from fresh rocks of different types and sampling was across intrusive/metavolcanic rock contact. Sample locations are summarised in (**Figure 2**). Thin and polished sections were prepared and studied under transmitted and reflected light microscopy at the Petrology Laboratory of the Geological Engineering Department, University of Mines and Technology (UMaT), Tarkwa using the Leica DM 2700P microscope. These minerals were identified and characterised based on their textural relationship taking into account mineral associations and alterations. Eight (8) representative and uniform samples were analysed for whole rock geochemistry at Associated Laboratory Services Minerals, Canada. Each sample was weighed, crushed using mechanical crusher to about 70 % below 2 mm and split using the riffle splitter. It was then pulverised using the agate mortar to about 85 % and made to pass through <75 μm to obtain powdered samples. From each powdered sample, glass discs were prepared using lithium borate flux composed of 50 % lithium tetraborate ($Li_2B_2O_7$) and lithium borate ($LiBO_2$). 0.9 g of ignited powdered samples were added to 9.0 g of lithium borate flux, mixed well and fused in an auto fluxer at about 1100˚C. From the molten melt, a flat pellet was prepared and subjected to X-ray fluorescence spectroscopy for major oxides using the XRF-06 equipment, the upper and lower limits being 100% and 0.01% respectively. For trace elements analysis, 0.2 g of each sample was digested using perchloric ($HClO_4$), nitric (HNO_3), hydrofluoric (HF) and hydrochloric (HCl) acids. The resultant constituents were topped up with dilute hydrochloric acid and analysed for trace elements using Inductively Coupled Plasma atomic emission spectroscopy (ICP-OES), correcting spectral inter-element interferences. The authenticity of the analytical procedure (from accuracy to standards) is obtainable at Associated Laboratory Services Minerals, Canada.

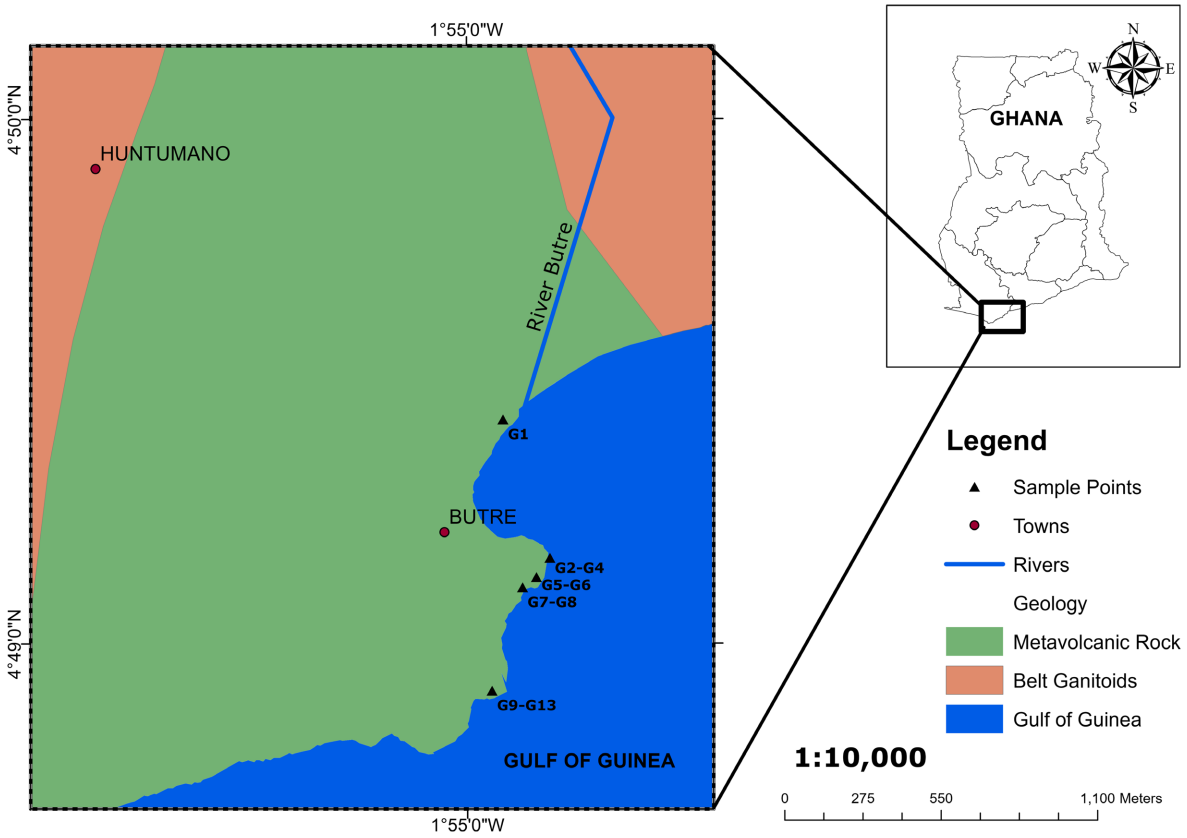

Figure 2. Geological Map of Study Area showing sample locations.

4. Petrography

4.1. Gabbro-Diorite

The rock is a coarse grained, weakly deformed porphyritic pod in metavolcanic rock which is cut by gabbro 2 (younger), containing granular plagioclase phenocrysts (Figure 3(a)). The matrix is made up of irregularly aligned medium grained plagioclase, quartz and amphiboles and shows chilled margin with metavolcanic rock (andesite). Medium grained version occurs as veins in host rocks with irregularly aligned porphyritic plagioclase in association with granular quartz and disseminated pyrite in quartzo-feldspathic veins occurring in the matrix (Figure 3(b) and Figure 3(c)).

In thin section, the rock is fine to medium grained, moderately foliated and porphyritic. Modal percentages of the minerals are shown in Table 1. A weak alignment of plagioclase is inter-foliated with amphiboles. Amphiboles are being replaced by opaque minerals with overprints of chlorites whiles plagioclase is overprinted by sericite (Figure 4(a)). A quartzo-feldspatic vein which is clouded by sericite almost completely replaces a fine to medium grained matrix, made up of plagioclase and amphibole (Figure 4(b)). Amphibole 2 which could be metamorphic occurs close to a quartzo-feldspatic intrusive whiles amphibole 3 appears to have come along with this same intrusive (Figure 4(c)). A weakly deformed intrusion of medium to coarse grained, irregularly aligned subhedral

plagioclase and amphibole that are strongly altered to fine sericite and epidote, respectively, occur in fine to medium grained matrix of plagioclase and amphibole may suggest two generations of diorite (diorite and gabbro-diorite) in relation to the cross cutting structure observed in the field (Figure 4(d)) and (Figure 4(e)). A cluster of aligned coarse grained, granular amphibole that is surrounded by fine grained, irregularly aligned amphibole and plagioclase suggest an amphibolite xenolith caught up by the rock. This coarse grained amphibole is overgrown by altered garnet (Figure 4(f)).

4.2. Diorite

In the field, the rock occurs as an intrusive in contact with metavolcanic rock (Figure 5(a)) with chill margins (Figure 5(b)) and as quartzo-feldspathic dyke (Figure 5(c)). In hand specimen, the rock is light green melanocratic, coarse grained and porphyritic. Plagioclase is granular and occurs as phenocrysts. The matrix is made up of irregularly aligned medium grained plagioclase, quartz and amphiboles.

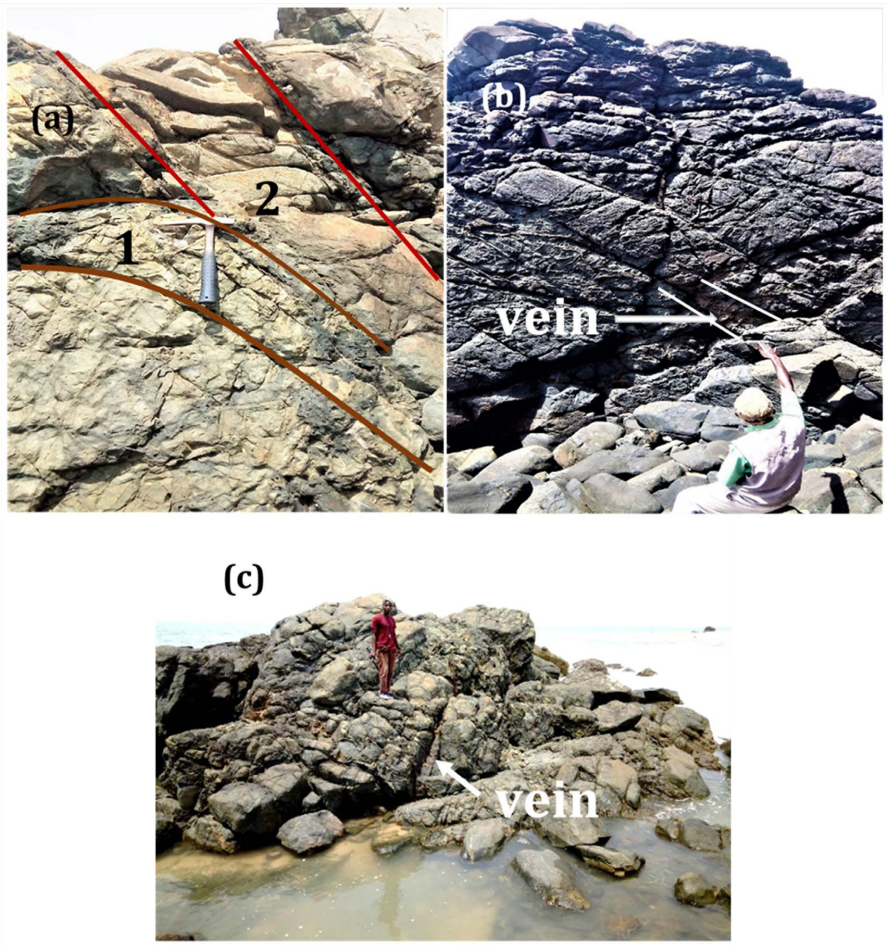

Figure 3. Field photographs showing: (a) Gabbro-diorite pod in metavolcanic rock, cut by diorite dyke. (b) Gabbro-diorite veins in fractured host rock. (c) Gabbro-diorite veins in pillow lava.

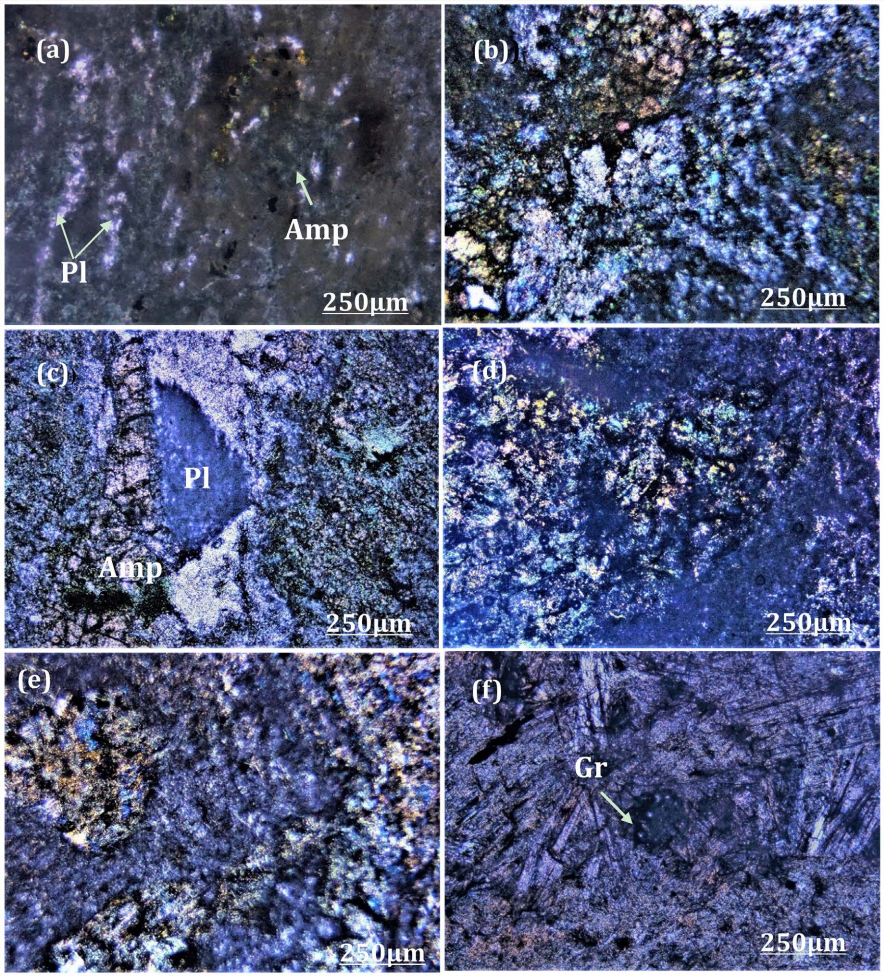

Figure 4. Photomicrographs of studied Gabbro-diorite showing: (a) Alignment of plagioclase and amphibole. (b) Quartzo-feldsparthic vein replacing rock. (c) Elongated amphibole in association with a quartzo-feldsparthic vein. (d and e) Intrusion of medium grained irregularly aligned amphibole and plagioclase into fine grained plagioclase and amphibole matrix. (f) Amphibolite xenolith with overgrown weathered garnet. Abbreviations, Plagioclase (Pl), Amphibole (Amp), Pyroxene (Px), Garnet (Gr), Sericite (Ser), Epidote (Epi), Tourmaline (Tur), Dolomite (Do), Pyrite (Py), Magnetite (Mag), Arsenopyrite (Apy), Pyrrhotite (Po).

In thin section, the rock is fine to medium grained and porphyritic made up of phenocrysts of carbonates and pyroxenes with irregular alignment of fine to medium grained subhedral amphiboles and plagioclase in the matrix. Modal percentages of the minerals are shown in Table 1. Carbonate phenocrysts in the rock is partially replaced by pyroxene. Pyroxene has inclusions of subhedral plagioclase that extincts at 15˚ (oligoclase composition) (Figure 6(a)). Dolomite phenocryst is partially replaced by epidote and plagioclase which show albite twinning at extinction angle of 37˚ (Figure 6(b)).

Later amphibole is coarse grained, granular, elongated and cuts foliation marked by fine grains of plagioclase and amphibole (Figure 6(c)). Other versions have undefined outlines but are replaced by earlier versions and later

Table 1. Modal Percentages of studied rocks from Butre area.

Mineral/ Sample ID	Gabbroic diorite			Diorite				Granodiorite
	G6	G8	G13	G3	G4	G7	G10	G14
Amphibole	48	41	55	32	32	36	40	30
Plagioclase	31	30	27	27	47.5	30	42	54.5
Pyroxene	-	10	-	20	5	-	-	-
Epidote	5	3	5	10	3	4	2	1
Sericite	5	5	-	5	6	5	5	5
Chlorite	5	10	6	4	5	10	5	5
Quartz	3	-	-	-	-	10	5	
Actinolite	2	-	-	-	-	-	-	-
Tourmaline	-	-	-	-	0.5	-	-	0.4
Apatite	-	-	-	-	-	-	-	2
Garnet	-	-	2	-	-	-	-	-
Pyrite	0.3	1	0.8	-	0.1	1.5	0.7	1.5
Arsenopyrite	0.5	-	4	1.75	0.7	3	0.1	-
Magnetite	0.2	-	0.15	0.25	0.1	0.5	0.2	0.5
Pyrrhotite	-	-	-	-	-	-	-	0.1
Gold	-	Trace	-	-	0.1	-	-	-
Limonite	-	-	0.05	-	-	-	-	-
Total	**100**	**100**	**100**	**100**	**100**	**100**	**100**	**100**

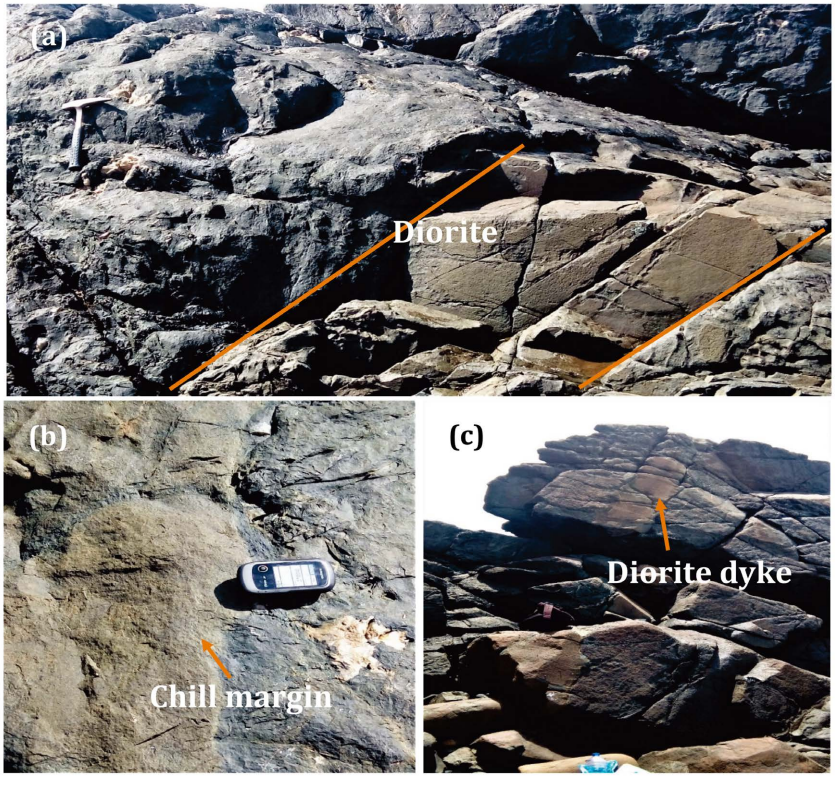

Figure 5. Field photographs showing: (a) Diorite intrusive into host metavolcanic rock. (b) Chill margin of intrusive and host metavolcanic rock. (c) Fractured diorite dyke in fractured host metavolcanic rock.

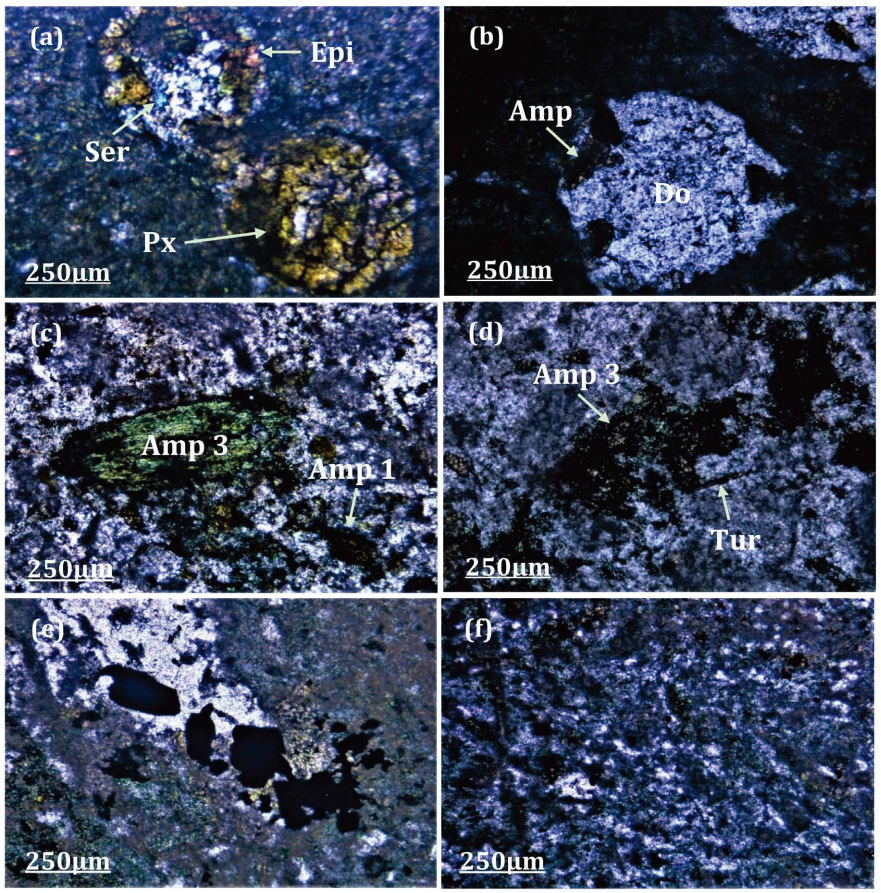

Figure 6. Photomicrographs of studied Diorite showing: (a) Carbonate phenocrysts overprinted by pyroxene, sericite and epidote. (b) Dolomite with overprints of amphibole at the edges. (c) Partially aligned plagioclase and amphibole with later overprint of coarse grained amphibole. (d) Coarse grained anhedral amphibole with later overprint of tourmaline. (e) Quartzo-feldsparthic vein overprinted by hydrothermal ore mineral. (f) Aligned amphibole and plagioclase due to shearing.

overprint of tourmaline (Figure 6(d)). Hydrothermal activity captured as hydrothermal opaque minerals overprint on amphibole, plagioclase and quartz (Figure 6(e)) whereas shearing has led to alignment of amphiboles and plagioclase (Figure 6(f)). Opaque minerals include pyrite and arsenopyrite that are partially replaced by magnetite and haematite. A cluster of anhedral pyrite is corroded by gangue mineral and partially replaced by spots of magnetite (Figure 7(a)). Elsewhere, pyrite is subhedral, isotropic, porphyroblastic and partially replaced by magnetite and exsolution of arsenopyrite (Figure 7(b)). Fine grained exsolution of arsenopyrite is overprinted by later arsenopyrite (Figure 7(c)). Also, blurry shaped pyrite is corroded by light gangue and pitted by magnetite infilling (Figure 7(d)).

4.3. Granodiorite

In the field, the rock is light green leucocratic, coarse grained with visible quartz, sulphides, porphyritic plagioclase and amphiboles and occurs as quartzo-felspatic

veins filling irregular fractures in andesite (Figure 8(a) and Figure 8(b)). In thin section, the rock is medium grained with moderate alignment of amphibole and plagioclase. Modal percentages are given in Table 1. Earlier amphiboles and plagioclase are parallel to foliation and overprinted by later amphiboles (Figure 9(a) and Figure 9(b)). Also, earlier fabrics of rock reveal the alignment of plagioclase and amphiboles (Figure 9(c)). Ore mineral include pyrite and magnetite. Pyrite is anhedral, isotropic and occurs in gangue. It is partially replaced by pyrrhotite and later magnetite (Figure 9(d)).

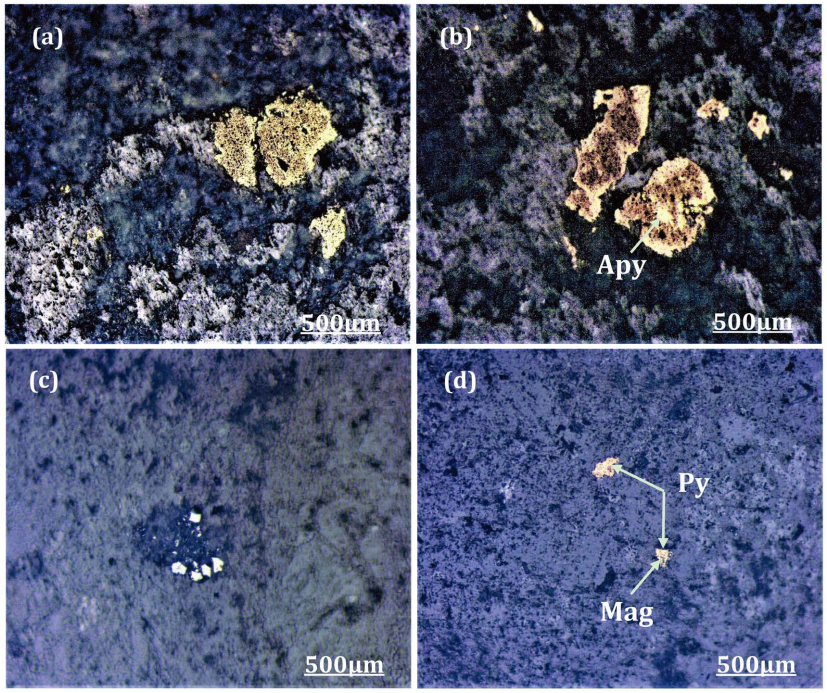

Figure 7. Photomicrographs of studied Diorite showing: (a) Anhedral pyrite with spots of magnetite. (b) Subhedral pyrite with partial overprint of magnetite and exsolution of arsenopyrite. (c) Fine grained exsolution of arsenopyrite with later overprints of arsenopyrite. (d) Blurbs of pyrite with infilling of magnetite.

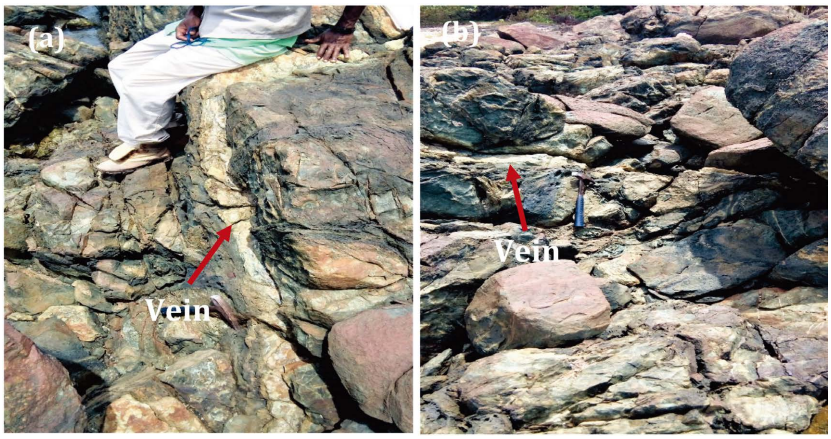

Figure 8. Field photographs showing: (a) and (b) Sheared granodiorite intrusive into host metavolcanic rock.

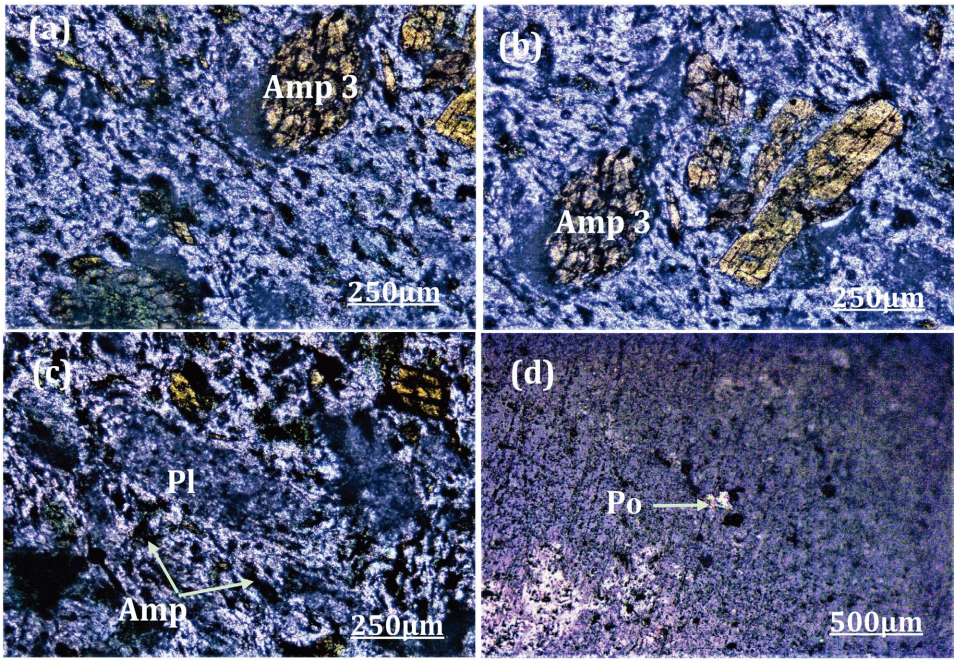

Figure 9. Photomicrographs of studied Granodiorite showing: (a) and (b) Alignment of fine to medium grained plagioclase and amphibole with overprint of later coarse grained amphiboles. (c) Earlier fabrics of rock with aligned plagioclase and amphiboles. (d) Anhedral pyrite partially replaced by pyrrhotite and magnetite.

5. Geochemistry

Results

Eight (8) representative samples were analysed at Associated Laboratory Services Minerals, Canada using X-ray fluorescence and Inductively Coupled Plasma Optical Emission Spectroscopy (ICP-OES). From whole rock geochemistry of rocks studied, the intrusives were grouped according to their silica content which ranges from (52.6 - 62.7 wt %). Whole rock geochemical results are presented in Table 2. Generally, Al_2O_3 is enriched for all rock types with range from (11.10 - 15.45 wt %). Na_2O is generally low in gabbro-diorite (0.13 - 1.94 wt %) but intermediate in diorite (2.78 - 4.11 wt %). CaO is high in gabbro-diorite (8.29 - 15.35 wt %) but generally low in diorite (3.03 - 6.95).

Total FeO is generally higher in gabbro-diorite (9.49 - 11.25 wt %) but low in diorite (5.56 - 9.28 wt %). Cr generally decreases from gabbro-diorite (470 - 590 ppm) to diorite (160 - 280 ppm). Rb is highest in diorite (59.3 ppm although a sample had lower Rb content of 0.4 ppm) and gabbro-diorite had (0.6 - 1.8 ppm). Zr is fairly enriched in diorite (109 ppm) although a sample recorded low Zr content of (60 ppm) but lower in gabbro-diorite (35 - 67 ppm). Line graphs of FeOT and CaO were plotted against SiO_2 to predict possible fractionation trend of the studied rocks (Figure 12). Trace elements triangular graphs to show the tholeiitic and calc-alkaline trends of the various rocks are also given (Figure 11(b)). Fractionation trend is supported in reverse by K_2O and Na_2O against SiO_2 wt % plots respectively (Figure 13).

Table 2. XRF analysis of intrusives from Butre area.

Major Oxide wt%	G3	G4	G6	G7	G8	G10	G13	G14
SiO_2	62.7	62.6	56.2	58.6	56.6	58.3	52.6	65
Al_2O_3	15.45	14.9	13.4	14.5	12.25	13.25	12.6	12.9
Fe_2O_3	5.56	5.84	10.4	8.09	9.49	9.28	11.25	7.15
CaO	3.03	4.69	15.35	6.95	8.29	5.76	13.35	12.65
MgO	2.87	3.57	2.21	4.16	7.5	7.38	5.19	0.89
Na_2O	3.95	4.11	0.13	3.79	1.94	2.78	0.23	0.39
K_2O	2.26	2.02	0.04	0.49	0.11	0.04	0.05	0.21
Cr_2O_3	0.033	0.032	0.064	0.022	0.062	0.044	0.085	0.058
TiO_2	0.46	0.46	0.82	0.67	0.5	0.52	0.86	0.42
MnO	0.08	0.09	0.11	0.1	0.14	0.12	0.13	0.06
P_2O_5	0.2	0.19	0.07	0.28	0.12	0.11	0.06	0.04
SrO	0.05	0.06	0.04	0.04	0.04	0.02	0.04	0.05
BaO	0.1	0.08	<0.01	0.02	0.01	<0.01	<0.01	0.01
LOI	3.32	1.74	1.48	1.98	2.65	3.49	2.49	1.38
Total	100.06	100.38	100.31	99.69	99.7	101.09	98.94	101.21
Trace Element (ppm)								
Ba	915	746	18.8	191	62.3	17.2	21.9	80.7
Ce	30.5	30.2	6.2	43.4	15.5	14.5	7.3	5.7
Cr	260	260	470	160	470	280	590	390
Dy	2.13	1.81	2.39	2.96	2.27	1.94	1.99	0.99
Er	1.13	1.02	1.62	1.41	1.2	1.19	1.19	0.61
Eu	0.96	0.87	0.46	1.32	0.73	0.62	0.73	0.36
Ga	20.3	19	16.1	17.3	14.7	10.5	12	14.8
Gd	2.58	2.52	1.97	3.61	2.08	1.85	2.12	1.01
Hf	3	2.8	0.8	3	1.8	1.5	1	0.7
Ho	0.39	0.37	0.47	0.57	0.44	0.45	0.46	0.28
La	14.9	14.5	3.3	20.4	6.9	6.5	2.9	2.9
Lu	0.15	0.15	0.27	0.25	0.19	0.19	0.18	0.09
Nb	3.3	3.2	1.6	3.3	2.2	2.2	2.6	1.5
Nd	14.7	14.2	5.6	24	8.4	8	5.9	3.8
Pr	3.82	3.89	1.02	5.86	2.08	1.85	1.03	0.76
Rb	59.3	55	0.6	8.4	1.8	0.4	0.7	3.9
Sm	2.98	3.07	1.79	4.61	2.1	2.08	2.02	1.09
Sr	436	486	379	365	328	150.5	356	417
Ta	0.3	0.4	0.2	0.4	0.3	0.2	0.3	0.2
Th	2.45	2.18	0.17	4.16	0.65	0.67	0.22	0.37
U	0.95	0.87	0.19	1.37	0.28	0.28	0.39	0.29
V	122	138	230	211	202	174	248	170
Yb	1.05	1.21	1.48	1.29	1.25	0.89	1.27	0.48
Zr	109	108	35	105	67	60	39	27

In thin section, chlorite and sericite alterations were observed. The general depletion of K_2O and enrichment of MgO and FeO_T in the rocks were investigated using the alteration index and the alteration box plot given by Ishikawa alteration index (AI) and the chlrorite-carbonate-pyrite index (CCPI). The Ishikawa alteration index is given by

$$\mathrm{AI} = \frac{100\left(\mathrm{K_2O} + \mathrm{MgO}\right)}{\mathrm{CaO} + \mathrm{MgO} + \mathrm{K_2O} + \mathrm{Na_2O}} \tag{1}$$

The chlorite-carbonate-pyrite index

$$\mathrm{CCPI} = \frac{100\left(\mathrm{MgO} + \mathrm{FeO}\right)}{\left(\mathrm{MgO} + \mathrm{FeO} + \mathrm{Na_2O} + \mathrm{K_2O}\right)} \tag{2}$$

The combination of some trace elements and major oxides were plotted against each other to predict probable tectonic settings and possible magma sources of the rocks (Figure 17 and Figure 18).

6. Discussion

The major rocks in the study area show massive to fractured and deformed pillow structures. These rocks were deduced to be basalt and andesite (Figure 10).

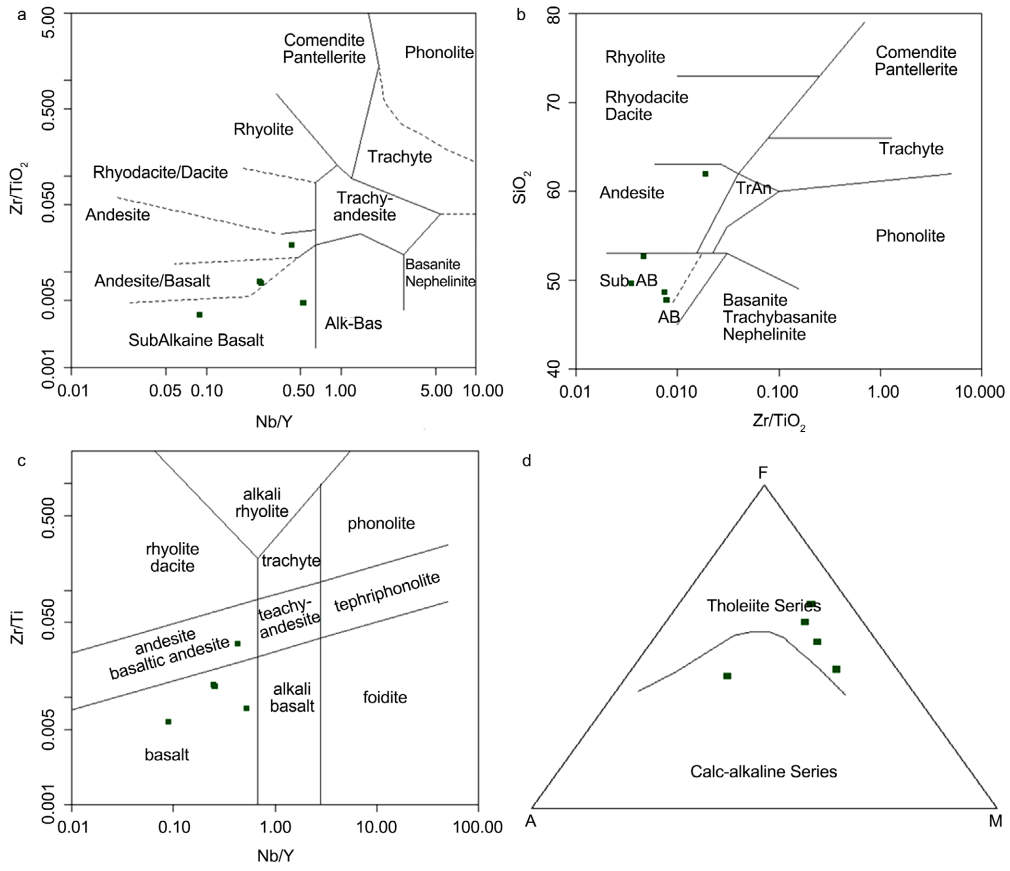

Figure 10. Classification diagrams of studied volcanic rocks showing: (a)Nb/Y against Zr/TiO_2, after Winchester & Floyd, 1977. (b) Zr/TiO_2 against SiO_2, after Winchester & Floyd, 1977. (c) Nb/Y against Zr/Ti after Pearce, 1996. (d) AFM diagram, after Irvine & Baragar, 1971.

According to Sylvester & Attoh (1992), pillows and massive lava flows occur at the middle of the volcanic section in the area. The major rocks are intruded by minor rocks of different thickness and textures which are medium to coarse grained and porphyritic with irregular alignment. A cross cutting structure observed in the field suggests generational relationship between the intrusives. Given their low quartz but high mafic mineral contents, the cross cutting intrusives (G6 and G7) were initially perceived as two generations of gabbro. Hence the first generation (G6) was given gabbro 1 and the later (G7) as gabbro 2. However, from geochemical plots, they were classified as gabbro-diorite (first generation) and diorite (second generation). The coarser grained and sheared intrusive (G14) which was previously diorite was also confirmed as granodiorite (**Figure 11(a)**). The primary minerals of the intrusives comprise of plagioclase of labradorite to andesine composition (An_{52} - An_{48}), amphibole and pyroxene

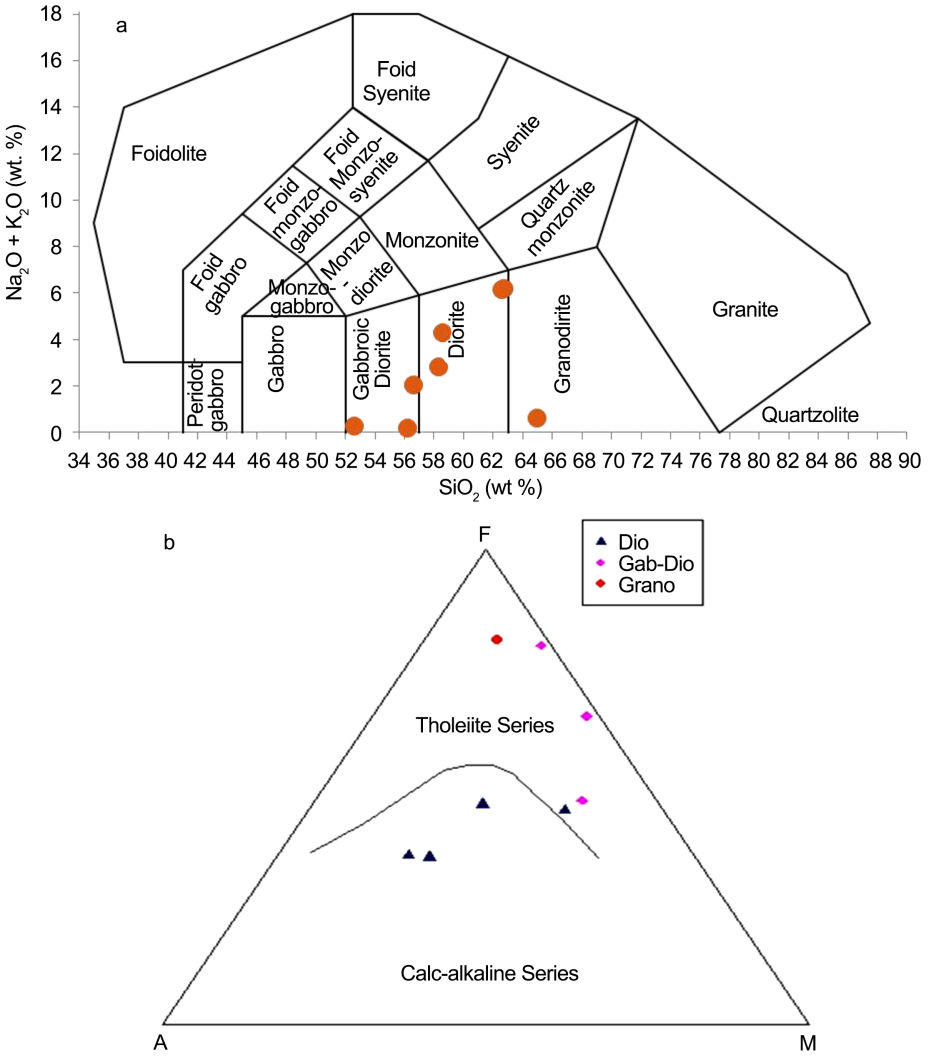

Figure 11. Geochemical discrimination plots of Intrusives from the study Area showing (a) Classification of intrusives by $Na_2O + K_2O$ against SiO_2, after Middlemost, 1994. (b) AFM diagram, after Irvine & Baragar, 1971.

with tourmaline, actinolite, apatite and garnet as accessory minerals. The gabbro-diorite is moderately foliated with primary fine grained plagioclase and amphiboles occupying the foliations. The diorite is porphyritic with medium to coarse grained plagioclase and amphiboles. The coarser grained granodiorite has aligned medium grained plagioclase and medium to coarse grained amphibole.

Generally, quartz, sericite and carbonate are alteration products of plagioclase. Amphibole is partially altered to chlorite and epidote. The gabbroic diorite which contains xenolith of amphibolite with overgrowth of garnet suggests an interaction with host rock during emplacement. John et al. (1999) are of the opinion that majority of the rocks within south of the Ashanti belt have been subjected to greenschist facies metamorphism; retrograde from amphibolite facies which is particularly observed in rocks near the belt granitoids.

In thin section, opaque minerals were seen overprinting amphiboles and in some cases, in quartzo-feldsparthic veins. Some of these opaque minerals could probably be alteration products of iron bearing silicates. Hatch et al. (1972) elaborated that opaque minerals, typically magnetite are generated from the conversion of amphibole to pyroxene which is facilitated by the decomposition of the hydroxyl group at elevated temperatures. The resulting opaque minerals may be as a result of oxidation and sulphidation of iron components of amphibole.

Both CaO and FeOT against SiO_2 show negative fractionation trends. FeO_T is enriched in all rock types but highest in gabbro-diorite (**Figure 12(a)**). CaO is enriched in gabbro-diorite and granodiorite but fairly enriched in diorite (**Figure 12(b)**).

K_2O and Na_2O against SiO_2, on the other hand, show positive fractionation trend with K_2O generally depleted in all rock types except two samples of diorite which were fairly enriched (**Figure 13(a)**). Na_2O is enriched in diorite but depleted in gabbro-diorite and granodiorite (**Figure 13(b)**). The characteristic < 0.5 wt. % K_2O content and the tholeiitic signature of the studied gabbro-diorite may suggest petrogenic features rather than alteration. According to Dampare et al. (2005) some mafic intrusives are typically hybrid rocks which may have formed by the interaction between granitoid magma and the host mafic rocks. Cr against SiO_2 show negative fractionation trend (**Figure 14(a)**) but Hf, Th and Nb show positive trends (**Figure 14(b)**, **Figure 15(a)** and **Figure 15(b)**) respectively. All rock types from this study are LREE depleted (La/Sm chondrite normalised ratios of gabbro-diorite = 0.9 to 2.05; diorite = 1.95 to 3.1; granodiorite = 1.66).

Diorite is fairly enriched in HREE (La/Yb chondrite normalised ratios of diorite = 4.96). Gabbro-diorite and granodiorite are depleted in HREE (La/Yb chondrite normalised ratios of gabbro-diorite = 1.51 to 3.75; granodiorite = 4.10). It is therefore postulated that the general fractionation trend is from tholeiitic gabbro-diorite, granodiorite and diorite (**Figure 13**).

The alteration box seeks to represent graphically alteration captured under two main indices; the Ishikawa alteration index (AI) and the chlrorite-carbonate-pyrite index (CCPI). These indices are useful in the determination of the extent of sericite and chlorite alteration defined by Ishikawa et al. (1976).

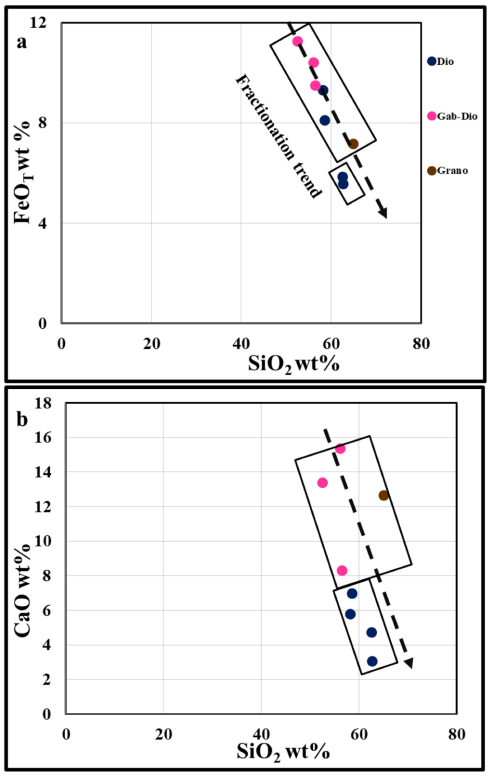

Figure 12. Binary Geochemical Plots of studied Intrusive showing variation of (a) FeO_T with SiO_2. (b) CaO with SiO_2.

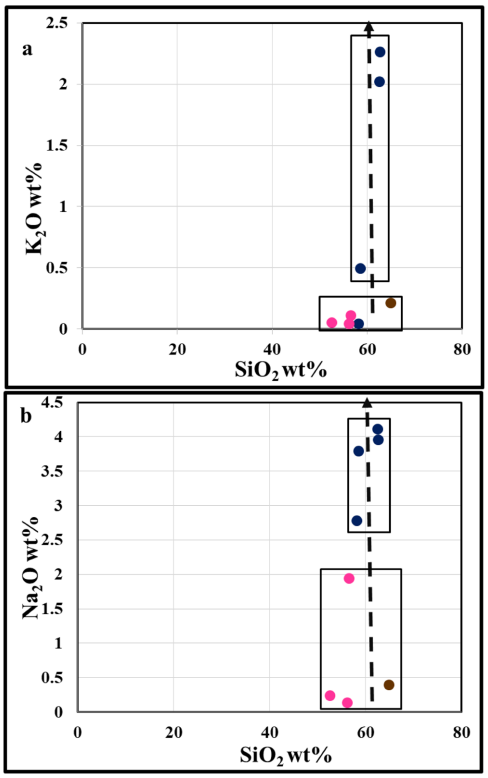

Figure 13. Binary Geochemical Plots of studied Intrusive showing variation of (a) K_2O with SiO_2, (b) Na_2O with SiO_2.

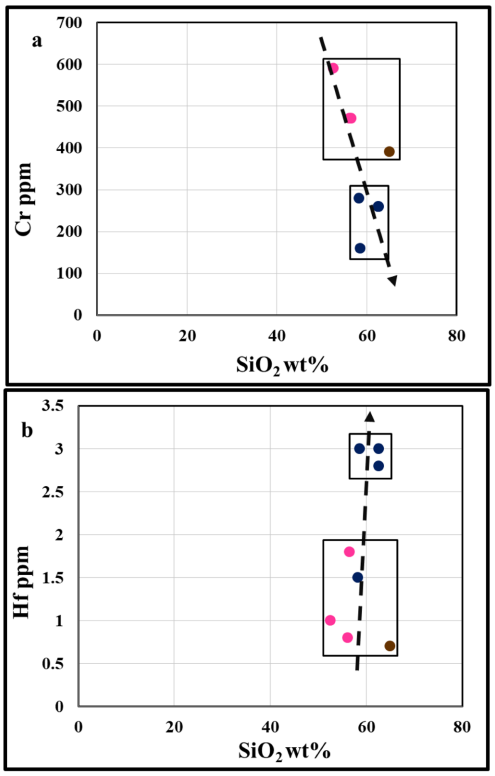

Figure 14. Binary Geochemical Plots of studied Intrusive showing fractionation trends of (a) Cr with SiO_2, (b) Hf with SiO_2.

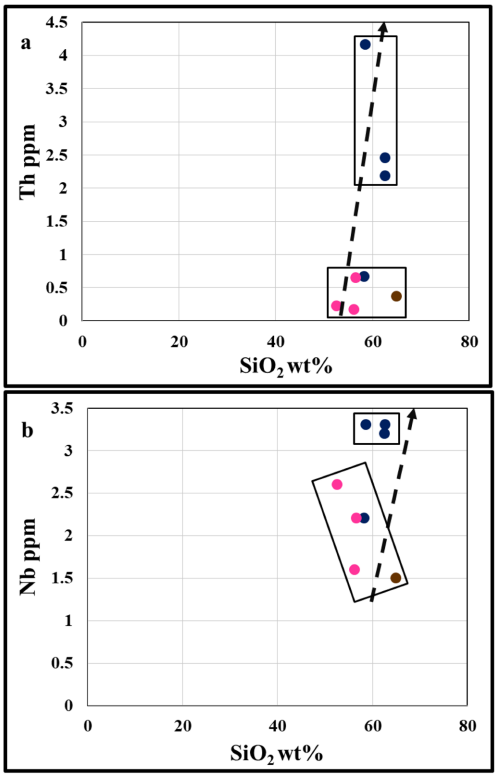

Figure 15. Binary Geochemical Plots of studied Intrusive showing fractionation trends of (a) Th with SiO_2, (b) Nb with SiO_2.

Figure 16(a) shows replacement of sodium (Na) in albite by potassium (K) in the formation of sericite (Eastoe et al., 1987) and Figure 16(b) shows a replacement of potassium (K) in sericite by magnesium (Mg) and iron (Fe) to form chlorite (Schardt et al., 2001). The CCPI was formulated by Large et al. (2001) to cater for two main limitations of the AI.

The AI does not consider carbonate alterations which usually lead to lower values in AI although the intensity of alteration is high and AI does not discriminate between sericite and chlorite alterations when used alone. Hence the index quantifies the increase in MgO and FeO_T linked to Mg-Fe chlorite formation with an additional advantage of its sensitivity to Mg-Fe carbonate alteration and magnetite and haematite enrichment.

In summary, the box plot suggests a general dolomite-ankerite-chlorite-calcite ± pyrite for gabbroic diorite, epidote-calcite-dolomite-ankerite for granodiorite and dolomite-ankerite-sericite ± epidote ± calcite for the diorite (Figure 16(c)). The chlorites are alteration products of amphibole and sericite after plagioclase feldspars related to greenschist facies metamorphism. Two types of metamorphism (amphibolite facies and greenschist facies) were determined. Amphibolite

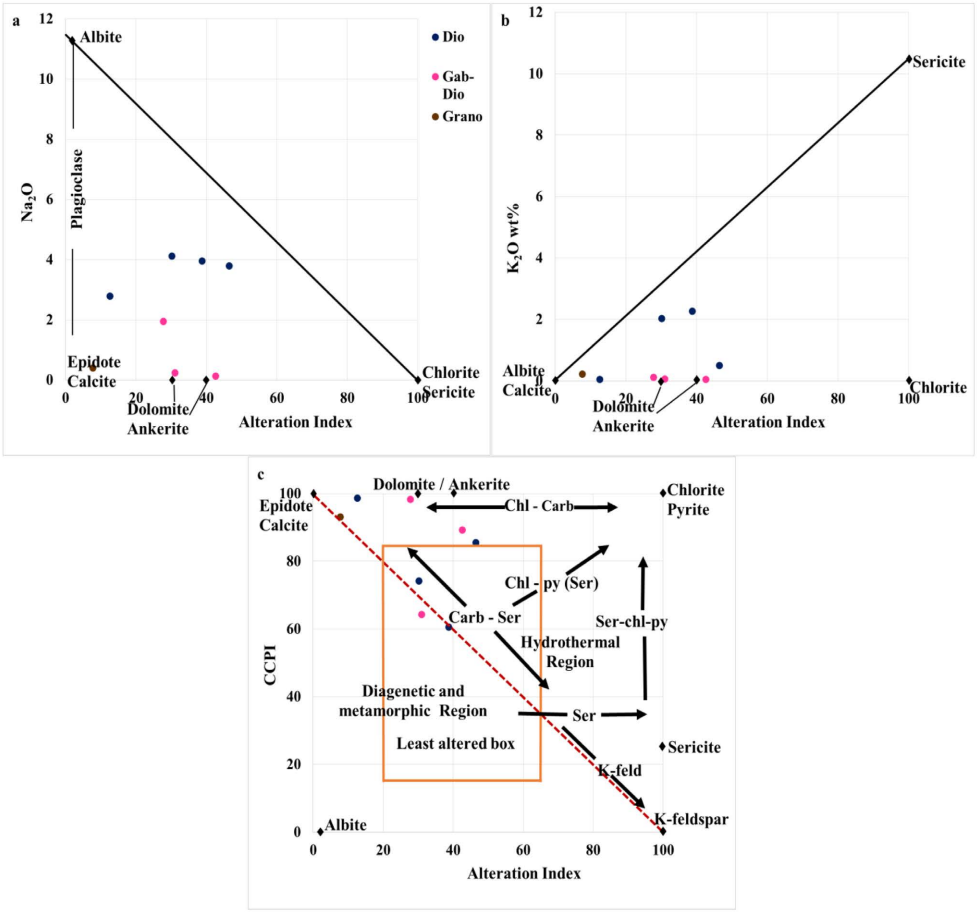

Figure 16. Alteration Box Diagrams showing (a) Trend of Na_2O wt% against Ishikawa Alteration Index (AI). (b) Trend of K_2O wt% against Ishikawa Alteration Index (AI). (c) Relationship between Ishikawa Alteration Index (AI) and CCPI index.

facies stage introduced amphibole + plagioclase + garnet + epidote + quartz + magnetite. The greenschist facies stage introduced minerals such as amphibole + epidote + chlorite + sericite + carbonate + haematite + pyrrhotite. Hydrothermal activity introduced carbonate + quartz + magnetite + pyrite.

The variation of K_2O, Na_2O, MgO, CaO with SiO_2 and Cr, Hf, Nb and Th with SiO_2 suggest the rocks are comagmatic and were emplaced in a volcanic island arc setting (Figure 17). However, gabbro-diorite and granodiorite were possibly deposited by mantle fractionates and diorite prior to plate collision (Figure 18).

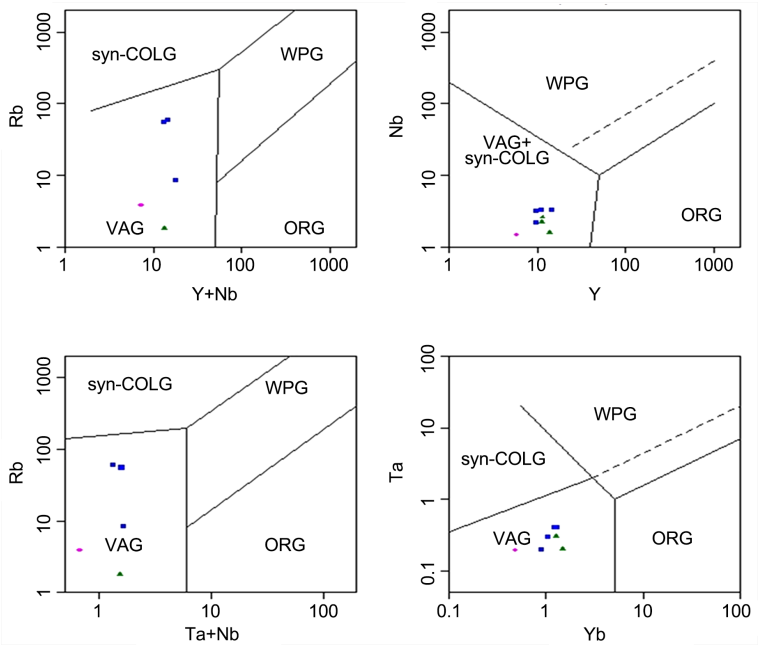

Figure 17. Tectonic Discrimination diagrams of studied Intrusive Rocks from Butre Area, after Pearce et al., 1984; Batchelor & Bowden, 1985.

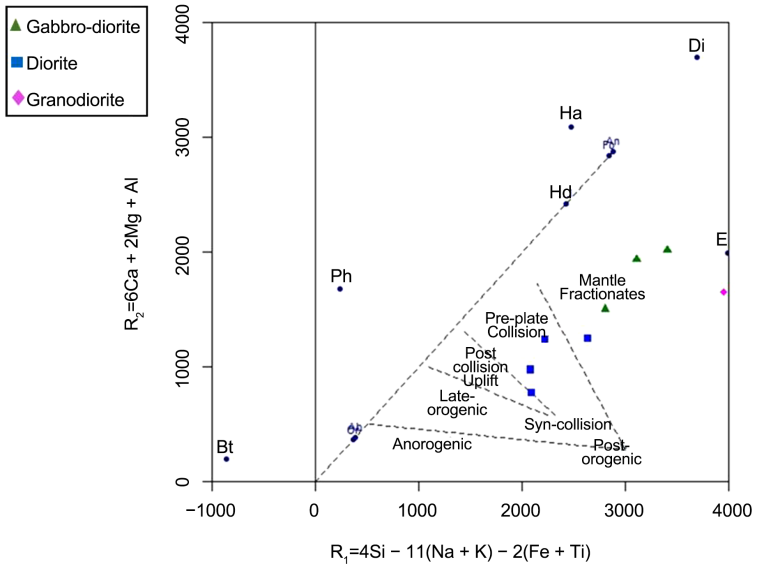

Figure 18. Possible sources of Magma of studied Intrusive Rocks from Butre Area, after Batchelor & Bowden, 1985.

7. Conclusion

The dykes at Butre area are gabbro-diorite, diorite, granodiorite comagmatically emplaced in a subduction zone into basalt and andesite on a tholeiitic differentiation trend from basalt through to diorite from mantle fractionates with diorite intrusion occurring before plate collision. Relict amphibolite facies metamorphism preceded greenschist facies. Arsenopyrite and pyrite accompanied the emplacement of diorite and granodiorite, respectively; earlier metamorphism introduced magnetite; haematite and pyrrhotite accompanied general metamorphism. The rocks are LREE depleted with La/Sm chondrite normalised ratios from 0.8 in basalt to 3.1 in diorite. There are also commonly negative anomalies of Eu and Ce with basalt, andesite and diorite weakly enriched in HREE with depletion in gabbroic diorite and granodiorite. The trace of gold in the lithologies is not surprising, as mineralisation in the Birimian of Ghana is associated with chloritisation, sericitisation carbonatisation and also composition of arsenopyrite, pyrite and pyrrhotite.

Future work should use microprobe analysis to examine mineralogy and its relationship to the stages of magma crystallisation. Fluid inclusion studies should aim at distinguishing hydrothermal from greenschist metamorphic alterations.

Conflicts of Interest

The authors declare no conflicts of interest regarding the publication of this paper.

References

Abouchami, W., Boher, M., Michard, A., & Albarede, F. (1990). A Major 2.1 Ga Event of Mantle Magmatism in West Africa, an Early Stage Crustal Accretion. *Geophysical Research Bulletin, 95,* 17605-17629. https://doi.org/10.1029/JB095iB11p17605

Allibone, A., Hayden, P., Cameron, G., & Duku, F. (2004). Paleoproterozoic Gold Deposits Hosted by Albite- and Carbonate-Altered Tonalite in the Chirano District, Ghana, West Africa. *Economic Geology, 99,* 479-497. https://doi.org/10.2113/gsecongeo.99.3.479

Amponsah, P. O., Salvi, S., Béziat, D., Baratoux, L., Siebenaller, L., Nude, P. M., Nyarko, R. S., & Jessell, M. W. (2015). Geology and Geochemistry of the Shear-Hosted Julie Gold Geposit, NW Ghana. *Journal of African Earth Sciences, 112,* 505-523. https://doi.org/10.1016/j.jafrearsci.2015.06.013

Amponsah, P. O., Salvi, S., Béziat, D., Baratoux, L., Siebenaller, L., Nude, P. M., Nyarko, R. S., & Jessell, M. W. (2016). The Bepkong Gold Deposit, Northwestern Ghana. *Ore Geology Reviews, 78,* 717-723. https://doi.org/10.1016/j.oregeorev.2015.06.022

Attoh, K., Evans, M. J., & Bickford, M. E. (2006). Geochemistry of an Ultramafic-Rodingite Rock Association in the Palaeoproterozoic Dixcove Greenstone Belt Southwestern Ghana. *Journal of African Earth Sciences, 45,* 333-346. https://doi.org/10.1016/j.jafrearsci.2006.03.010

Batchelor, R. A., & Bowden, P. (1985). Petrogenetic Interpretation of Granitoid Rock Series Using Multicationic Parameters. *Chemical Geology, 48,* 43-55. https://doi.org/10.1016/0009-2541(85)90034-8

Berge, J. (2011). Paleoproterozoic, Turbidite-Hosted, Gold Deposits of the Ashanti Gold Belt (Ghana, West Africa): Comparative Analysis of Turbidite-Hosted Gold Deposits and an Updated Genetic Model. *Ore Geology Reviews, 39,* 91-100. https://doi.org/10.1016/j.oregeorev.2010.12.001

Craw, D., & Findlay, R. H. (1984). Hydrothermal Alteration of Lower Ordovician Granitoids and Devonian Beacon Sandstone at Taylor Glacier, McMurdo Sound, Antarctica. *New Zealand Journal of Geology and Geophysics, 27,* 465-475. https://doi.org/10.1080/00288306.1984.10422266

Dampare, S. B., Shibata, T., Asiedu, D. K., Osae, S., & Banoeng-Yakubo, B. (2008). Geochemistry of Paleoproterozoic Metavolcanic Rocks from the Southern Ashanti Volcanic belt, Ghana: Petrogenetic and Tectonic Setting Implications. *Precambrian Research, 162,* 403-423. https://doi.org/10.1016/j.precamres.2007.10.001

Dampare, S., Shibata, T., Asiedu, D., & Osae, S. (2005). Major-Element Geochemistry of Proterozoic Prince's Town Granitoid from the Southern Asbanti Volcanic Belt, Ghana. *Okayama University. Earth Science Reports, 12,* 15-30. http://ousar.lib.okayama-u.ac.jp/files/public/1/13853/20160527201125250859/ESR_12_15.pdf

Eastoe, C. J., Solomon, M., & Walshe, J. L. (1987). District-Scale Alteration Associated with Massive Sulphide Deposits in the Mount Read Volcanics, Western Tasmania. *Economic Geology, 82,* 1239-1258. https://doi.org/10.2113/gsecongeo.82.5.1239

Eisenlohr, B. N., & Hirdes, W. (1992). The Structural Development of the Early Proterozoic Birimian and Tarkwaian Rocks of Southwest Ghana, West Africa. *Journal of African Earth Sciences, 14,* 313-325. https://doi.org/10.1016/0899-5362(92)90035-B

Griffis, R. J., Barning, K., Agezo, F. L., & Akosah, F. K. (2002). *Gold Deposits of Ghana* (pp. 7-12, 19-37, 163-169). Minerals Commission Report, Accra.

Hatch, F. K., Wells, A. K., & Wells, M. K. (1972). *Petrology of the Igneous Rock* (13th ed., pp 98-99). George Allen & Unwin Ltd.

Hirdes, W., Davis, D. W., & Eisenlohr, B. N. (1992). Reassessment of Proterozoic Granitoid Ages in Ghana on the Basis of U/Pb Zircon and Monazite Dating. *Precambrian Research, 56,* 89-96. https://doi.org/10.1016/0301-9268(92)90085-3

Hirdes, W., Senger, R., Adjei, J., Efa, E., Loh, G., & Tettey, A. (1993). Explanatory Notes for the Geological Map of Southwest Ghana—1:100,000 (Wiawso, Asafo, Kukuom, Sunyani and Berekum Sheets). *Geologisches Jahrbuch Reihe B, 83,* 139 p.

Irvine, T. N., & Baragar, W. R. A. (1971). A Guide to the Chemical Classification of the Common Volcanic Rocks. *Canadian Journal of Earth Sciences, 8,* 523-548. https://doi.org/10.1139/e71-055

Ishikawa, Y., Sawaguchi, T., Iwaya, S., & Horiuchi, M. (1976). Delineation of Prospecting Targets for Kuroko Deposits Based on Modes of Volcanism of Underlying Dacite and Alteration Halos. *Mining Geology, 26,* 105-117.

John, T., Kleimd, R., Hirdes, W., & Loh, G. (1999). The Metamorphic Evolution of the Palaeoproterozoic (Birimian) Volcanic Ashanti Belt (Ghana, West Africa). *Precambrian Research, 98,* 11-30. https://doi.org/10.1016/S0301-9268(99)00024-8

Kaur, P., Chaudril, N., Hoffman, A. W., Raczek, I., Okrusch, M., Skora, S., & Baumgartner, P. (2012). Two-Stage, Extreme Albitisation of A-Type Granite from Rajasthan, NW India. *Journal of Petrology, 53,* 919-948. https://doi.org/10.1093/petrology/egs003

Kesse, G. (1985). *The Mineral and Rocks Resources of Ghana* (p. 609). A.A. Balkema.

Kumral, M., Abdelnasser, A., & Budakoglu, M. (2016). Geochemistry of Hydrothermal Alteration Associated with Cenozoic Intrusion-Hosted Cu-Pb-Zn Mineralization at

Tavşanlı Area, Kütahya, NW Turkey. *Minerals, 6,* Article 13. https://doi.org/10.3390/min6010013

Large, R., Gemmell, J. B., Paulick, H., & Huston, D. L. (2001). The Alteration Box Plot: A Simple Approach to Understanding the Relationship between Alteration Mineralogy and Lithogeochemistry Associated with Volcanic-Hosted Massive Sulphide Deposits. *Economic Geology, 96,* 957-971. https://doi.org/10.2113/gsecongeo.96.5.957

Leube, A., Hirdes, W., Mauer, R., & Kesse, G. (1990). The Early Proterozoic Birimian Supergroup of Ghana and Some Aspects of Its Associated Gold Mineralisation. *Precambrian Research, 46,* 139-165. https://doi.org/10.1016/0301-9268(90)90070-7

Loh, G., & Hirdes, W. (1999). Explanatory Notes for the Geological Map of Southwest Ghana. 1:100,000: Sheets Sekondi (0402A) and Axim (0403B). *Bulletin of Ghana Geological Survey, 49,* 149. (Unpublished)

Micko, J., Tosdal, J., Bissig, T., & Chamberlain, C. (2014). Hydrothermal Alteration and Mineralisation of the Galore Creek Alkalic Cu-Au Porphyry Deposit, Northwest British Columbia, Canada. *Economic Geology, 109,* 891-914. https://doi.org/10.2113/econgeo.109.4.891

Middlemost, E. A. K. (1994). Naming Materials in the Magma/Igneous Rock System. *Earth-Sciences Reviews, 37,* 215-224. https://doi.org/10.1016/0012-8252(94)90029-9

Oberthür, T, Vetter, U., Davis, D. W., & Amanor, J. A. (1998). Age Constraints on Gold Mineralisation and Paleoproterozoic Crustal Evolution in the Ashanti Belt of Southern Ghana. *Precambrian Research, 89,* 129-143. https://doi.org/10.1016/S0301-9268(97)00075-2

Oberthür, T., Hirdes, W., Höhndorf, A., Mumm, A. S., Vetter, U., Weiser, T., Davis, D. W., Blenkinsop, T. G., Amanor, J. A., & Loh, G. (1995). A Review of Gold Mineralisation in the Ashanti Belt of Ghana and its Relation to the Crustal Evolution of the Terrane. *Communications of the Geological Survey of Namibia, 10,* 121-127.

Pearce, J. A. (1996). A User's Guide to Basalt Discrimination Diagrams. In D. A. Wyman (Ed.), *Trace Element Geochemistry of Volcanic Rocks: Applications for Massive Sulphide Exploration* (pp. 79-113). Geological Association of Canada.

Pearce, J. A., Harris, N. B. W., & Tindle, A. G. (1984). Trace Element Discrimination Diagrams for the Tectonic Interpretation of Granitic Rocks. *Journal of Petrography, 25,* 956-983. https://doi.org/10.1093/petrology/25.4.956

Perrouty, S., Aillères, L., Jessell, M. W., Baratoux, L., Bourassa, Y., & Crawford, B. (2012). Revised Eburnean Geodynamic Evolution of the Gold-Rich Southern Ashanti Belt, Ghana, with New Field and Geophysical Evidence of Pre-Tarkwaian Deformations. *Precambrian Research, 204-205,* 12-39. https://doi.org/10.1016/j.precamres.2012.01.003

Rajah, S. S., Fateh, C., & Singh, S. D. (1977). The Granitoids and Mineralisation of the Eastern Belt of Penisula Malaysia. *Geological Society of Malaysia Bulletin, 9,* 209-232. https://doi.org/10.7186/bgsm09197715

Salvi, S., Ofori Amponsah, P., Siebenaller, L., Béziat, D., Baratoux, L., & Jessell, M. (2015). Shear-Related Gold Mineralisation in Northwest Ghana: The Julie Deposit. *Ore Geology Reviews, 78,* 712-717. https://doi.org/10.1016/j.oregeorev.2015.08.008

Schardt, C., Cooke, D. R., Gemmell, J. B., & Large, R. R. (2001). Geochemical Modeling of the Zoned Footwall Alteration Pipe, Hellyer Volcanic-Hosted Massive Sulphide Deposit, Western Tasmania, Australia. *Economic Geology, 96,* 1037-1054. https://doi.org/10.2113/gsecongeo.96.5.1037

Smith, A. J. B., Henry, G., & Frost-Killian, S. (2016). A Review of the Birimian Supergroup- and Tarkwaian Group-Hosted Gold Deposits of Ghana. *Episodes, 39,* 177-197.

https://doi.org/10.18814/epiiugs/2016/v39i2/95775

Sylvester, P. J., & Attoh, K. (1992). Lithostratigraphy and Composition of 2.1 Ga Greenstone Belts of the West African Craton and Their Bearing on Crustal Evolution and the Archean-Proterozoic Boundary. *Journal of Geology, 100,* 377-393. https://www.jstor.org/stable/30065738 https://doi.org/10.1086/629593

Tetteh, G. M., & Effisah-Otoo, E. (2017). Petrography and Geochemistry of Some Granitoids Associated with Gold Mineralisation at Mpohor Area in Southeastern Ashanti Belt of the Birimian, Ghana. *Ghana Mining Journal, 17,* 31-42. https://doi.org/10.4314/gm.v17i1.4

Winchester, J. A., & Floyd, P. A. (1977). Geochemical Discrimination of Different Magma Series and Their Differentiation Products Using Immobile Elements. *Chemical Geology, 20,* 325-343. https://doi.org/10.1016/0009-2541(77)90057-2

Wright, J. B., Hastings, D. A., Jones, W. B., & Williams, H. R. (1985). *Geology and Mineral Resources of West Africa*. Allen and Unwin.

Yao, Y., & Robb, L. J. (2000), Gold Mineralisation in Palaeoproterozoic Granitoids at Obuasi, Ashanti Region, Ghana: Ore Geology, Geochemistry and Fluid Characteristics. *South African Journal of Geology, 103,* 255-278. https://doi.org/10.2113/1030255